Solid phase formation of silicon nanocrystals by bulk ultrafast laser–matter interaction

Amir H. Nejadmalayeri,[1,4,*] Philip Scrutton,[1] Jacky Mak,[1] Amr S. Helmy,[1] Peter R. Herman,[1] Jonas Burghoff,[2] Stefan Nolte,[2] Andreas Tünnermann,[2] and Jörg Kaspar[3]

[1]*Photonics Group, Department of Electrical and Computer Engineering and Institute for Optical Sciences, University of Toronto, 10 King's College Road, Toronto, Ontario M5S 3G4, Canada*
[2]*Institut für Angewandte Physik, Friedrich-Schiller-Universität Jena, Max-Wien-Platz 1, 07743 Jena, Germany*
[3]*Fraunhofer-Institut für Werkstoff und Strahltechnik, Winterbergstraße 28, 01277 Dresden, Germany*
[4]*Present address, Research Laboratory of Electronics, Massachusetts Institute of Technology, Cambridge, Massachusetts 02139, USA*
**Corresponding author: nejadmal@mit.edu*

Received July 5, 2007; revised October 22, 2007; accepted November 5, 2007;
posted November 9, 2007 (Doc. ID 84912); published December 3, 2007

Ultrashort pulse laser interaction with silica–silicon interfaces is presented as a means for *all-solid-phase* formation of high-purity silicon nanoparticles in the absence of ablation plumes or any substrate intermixing with surfaces in ambient air. Transmission electron microscopy and Raman spectroscopy provide definitive evidence for creation of nanocrystals in the silica host, while compressive stress in the silicon substrate corroborates the formation of optical waveguides parallel to the tracks. © 2007 Optical Society of America

OCIS codes: 320.7120, 160.4236, 300.6450, 140.3330, 350.3390, 320.7160.

Recent demonstrations of Raman lasing [1] and parametric amplification [2] have stimulated widespread interest in bulk crystalline silicon (Si) photonics. There has also been significant parallel progress in obtaining net optical gain [3] and laser emission (at cryogenic temperatures) [4] from the nanocrystalline form of Si since the first photoluminescence observations [5,6]. The formation of photoactive Si nanocrystals (NCs) poses several fabrication challenges that have been met with varying success by techniques such as laser annealing [7], electrochemical etching [6], laser ablation [8], and ion implantation [3]. These methods share a common disadvantage in generating NCs on the surface or shallowly embedded into the bulk. This Letter presents a means of producing Si NCs deep below the surface—in the absence of chemicals, contaminants, and ablation plumes—that promises significant improvements in the elemental purity, quality, and associated optical properties of NCs.

During the past decade, the interaction of ultrashort laser pulses with the bulk of transparent materials has been extensively studied. These processes can form microvoids, microcracks, color centers, refractive index changes, and nanogratings [9–12]. Although the earlier studies were focused on SiO_2-based materials, we recently extended the technique to Si [13], wherein we inscribed optical waveguides.

To our knowledge, this Letter reports the first observation of an all-solid-phase phenomenon, the laser generation of nanocrystals (NCs) within bulk transparent media. Here, we present microscopic and spectroscopic analyses of the samples treated by ultrashort pulses in the proximity of the $Si-SiO_2$ interface to ascertain the nature of the laser modifications and provide concrete evidence for the formation of Si NCs. We also quantitatively estimate the built-in compressive stress in the Si matrix that explains the origin of the refractive index increase, which is responsible for waveguide formation.

The sample preparation procedure was similar to the waveguide writing approach described in [13]. In summary, mid-IR ultrafast radiation of 2400 nm was selected with photon energy less than half the bandgap to propagate in the transparency window of Si. Linearly polarized light was focused with a Schwarzschild objective (NA=0.5) into the sample and scanned transversely by using a motorized translation stage. In this study, the samples were Si wafers overcoated with 20 μm thick oxide. Laser exposure created damage tracks along the [100] crystal direction at the $Si-SiO_2$ interface, leaving the top oxide surface intact. The laser modifications also created optical waveguides on both sides of the track, which guided both 1300 and 1550 nm, with moderate losses of $\approx$1 dB/cm.

To study these laser-induced modifications in detail, we performed two complimentary studies, transmission electron microscopy (TEM) and Raman spectroscopy.

Figure 1 shows TEM images and diffraction patterns recorded near the $Si-SiO_2$ interface following 1 kHz rate exposure of $\approx$4.5 μJ pulses. The sample was scanned at a speed of 100 μm/s parallel to the laser polarization. Small crystallites are clearly vis-

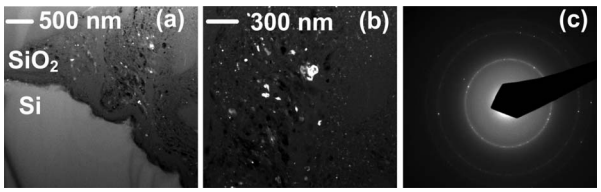

Fig. 1. Dark field TEM images of the laser-structured region: (a) at the interface between Si crystal (lower left) and oxide layer (upper right) showing randomly orientated Si nanoparticles (bright dots) in the silica layer and (b) higher magnification image of this molten oxide region with silicon nanocrystals. (c) Electron diffraction pattern of (b).

ible in Fig. 1(a) within the amorphous oxide (top right) immediately above the silicon–glass interface. The magnified image of this region as shown in Fig. 1(b) illustrates that the crystallites exhibit a variety of submicrometer sizes and that their spatial distribution does not have any particular order. By recording TEM pictures similar to Fig. 1(a) under different illumination angles, one observes that only a small number of spots become bright at any specific angle, an indication of both the existence and the random orientation of crystallites. Alternatively, the discrete nature of the diffraction rings in Fig. 1(c) is the evidence of Si NCs, while their random orientation is manifested in the uniformity of the rings. The size of the majority of the silicon particles was estimated to be in the range 5–30 nm. However, several larger crystallites with dimensions of ≈100 nm were found. Additionally, a few small pores were observed in the region containing the silicon particles. These pores are evidence that the oxide was in the transient state of an overheated melt during the laser interaction.

The following picture can be deduced from the TEM analysis: although Si and SiO_2 are both linearly transparent to the exploited laser radiation, the interface exhibits a relatively low damage threshold due to impact ionization [14] and/or other nonlinear interactions. These processes cause a rapid heating of a thin Si layer at the interface, which results in the rapid melting of the crystal followed by the adjacent oxide. Since thermal diffusivity of Si is 2 orders of magnitude larger than that of glass, the heat is mostly contained within the glass; henceforth the bulk of the melt is formed in the glass. The explosive laser interactions therefore only drive a thin layer of Si melt into the glass melt, resulting in the mixture of both components mainly in the silica layer (Fig. 1). Upon cooling, the molten glass resolidifies, and the silicon droplets recrystallize, forming a heterogeneous mixture of Si particles of nanoscale size, randomly oriented and positioned in the glass.

To further assess the NCs, Raman spectroscopy was applied in the backscattering configuration inside the laser-exposed zone. The sample undergoing Raman analysis was fabricated with the same conditions used to form waveguides in [13], namely, a pulse energy of ≈1.7 μJ and a velocity of 33 μm/s perpendicular to the laser polarization. After exposure, the edge facets were polished to optical quality and analyzed about the Si/SiO_2 interface, near the laser-formed waveguide tracks. Typical Raman spectra recorded from the SiO_2 side of the laser-modified zone at low and high excitation powers are plotted in Fig. 2(a) and 2(b), respectively.

The shifts in spectral width, asymmetry, and peak position were interpreted following Xia *et al.* [15] and divided into three classes of Si structure identified as amorphous-like (a-band) for bands close to 480 cm^{-1}, stressed c-Si and/or the core part of Si NCs (c-band), close to 521 cm^{-1}, and the shell of Si NCs (s-band) for bands between these other two. The Raman signal from this last band depends on the structure of the shell, including thickness, area and whether it is oxidized, passivated, or formed of dangling bands.

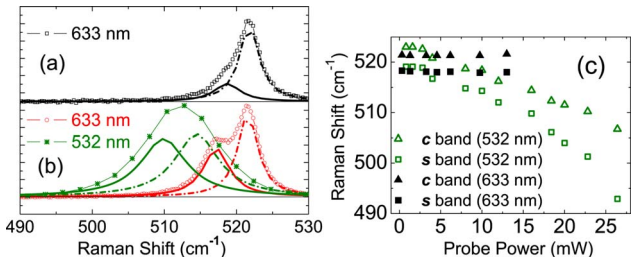

Fig. 2. (Color online) Typical Raman spectra excited inside the modified glass zone with (a) low-power 633 nm and (b) high-power 633 and 532 nm laser light, together with fitted s-band (solid) and c-band (dotted-dashed) spectra. (c) Spectral shifts of these isolated c- and s-bands are plotted as functions of 532 and 633 nm excitation power.

Compared with c- and s-band emissions in Figs. 2(a) and 2(b), the a-band emissions were weak in our samples and appeared unresolved. Therefore, the Raman analysis was centered on line fitting to asses the relative contribution of c- and s-bands, generating the isolated band profiles shown, respectively, as solid and dotted–dashed curves below each spectral envelope in Fig. 2(a) and 2(b). Spectral shifts here directly reflect the local stress in bulk c-Si, while NCs introduce shifts as well as asymmetry and broadening of the peak [16]. One can then differentiate between these two effects and obtain quantitative information about the stress from the collected Raman spectra.

However, to ensure that other effects, such as localized heating by the pump laser, do not unduly influence or mask the primary Raman response of NCs [17,18], spectral shifts of both the c- and s-bands were assessed as a function of power for both 633 and 532 nm pump lasers. The observed spectral shifts, plotted in Fig. 2(c), are more pronounced for the shorter wavelength source (532 nm)—owing to higher absorption in Si—while laser heating drives a nonlinear power dependence of the s-band peak position. In contrast, the peak positions of the c- and s-bands are almost independent of power at the 633 nm wavelength, and even the rapidly shifting c-band follows a linear dependence on the 532 nm probe power. As a result, high-power probes at short wavelengths are preferable for qualitative analysis, since the effect of the crystallites will be magnified because of a strong power dependency, while for quantitative analysis long-wavelength excitation at low power is necessary.

Raman responses from the bulk silicon immediately below the laser-modified zone were dominated by c-band emissions under low-power 633 nm laser excitation. Blueshifts of $\Delta\nu \approx 1.1$, 1.0, 0.5 cm^{-1} were observed at positions 5, 10, and 50 μm below the interface, which correspond to planar compressive stresses of $\sigma \approx 2.7$, 2.5, 1.3 kilobars (1 kilobar = 100 MPa), respectively, according to the relation given in [16],

$$\sigma = -2.49\Delta\nu, \tag{1}$$

and assuming there is no stress along the [010] direction due to symmetry. In Eq. (1), σ is the stress (in

kilobars) and $\Delta\nu$ (in reciprocal centimeters) is the peak shift of the Raman line with respect to the unperturbed c-Si.

The compressive stress conforms with the results of TEM analysis, showing stress in the Si matrix near the modified zone—manifested in dark contours in the c-Si region of Fig. 1(a). Further, the optical waveguiding that we reported [13] can then be associated with the increase of refractive index due to the density increase induced by this compressive stress.

Areal maps of the Raman emission were collected point by point by scanning a 12 mW 532 nm laser beam over a 7×10.6 μm^2 area of the laser-modified facet in 200 nm steps. The Raman spectrum in the range of 475–525 cm^{-1} could be binned into three different spectral ranges of 475–490, 490–515, and 515–525 cm^{-1}, corresponding to the *a*-, *s*-, and *c*-band, respectively. The normalized intensity of the deconvolved peaks in the *c*- and *s*-band are plotted in false color in Figs. 3(a) and 3(b), respectively.

The strong presence of *c*-band emission over a 4×22 μm^2 area in Fig. 3(a) further confirms the localized compressive stress and disorder that enhance the Raman response in the Si substrate below the laser-modified tracks. On the other hand, the high-intensity islands in Fig. 3(b), associated with the *s*-band, identify clusters of Si NCs formed in the glass matrix that are qualitatively similar to the distribution of NCs identified in Fig. 1(a), despite the different laser exposure conditions—orthogonal polarizations and slightly different total fluence—used to fabricate the TEM and Raman samples.

The conclusion obtained from this analysis is that the Si matrix close to the modified region is disordered and under stress, hence causing stronger *c*-band peaks compared with the pristine Si. On the other hand, in the modified glass zone, Si is in the form of NCs embedded into the glass matrix, having a distribution of sizes, manifested in the variation of shifted *c*-band peak shifts, accompanied by strong *s*-band peaks, characteristic of the NCs' shells. Whether this phenomenon is a unique characteristic of the ultrashort pulsed laser interaction with the $Si-SiO_2$ system or whether it can occur in other systems such as Si/Si_3N_4 will be the subject of future research.

In summary, TEM and Raman spectroscopy have provided definitive evidence for the formation of silicon nanocrystals when a silicon–silica interface is exposed to mid-IR ultrafast laser radiation. This is the first time to our knowledge that laser interaction has been exploited to form NCs in the bulk, where the all-solid-phase dynamics present the unprecedented advantage of a clean environment for NC formation in the absence of chemicals, contaminants, or ablation plumes. These results suggest research directions toward understanding and applying bulk ultrafast laser–matter interactions.

Of further significance is the close proximity (<10 μm) of the nanocrystals seen in Raman spectra here to the evanescent fields that were observed [13] in structures formed with identical laser-exposure conditions. Considering the attractive luminescence properties—now under study for the present Si NCs—their proximity to such guided wave optics in a single-step process suggests new opportunities to explore means of making compact Si-based light sources.

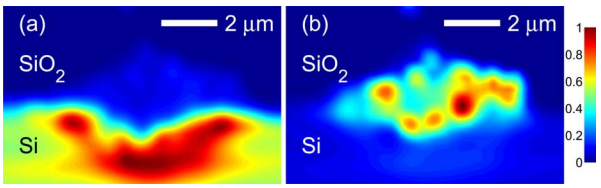

Fig. 3. (Color online) The 2D maps of Raman peak shifts for (a) *c*-band, (b) *s*-band. The maps are coded in normalized pseudocolor, where dark blue to dark red colors represent low- (0.0) to high- (1.0) intensity Raman lines.

This work was supported by the Natural Sciences and Engineering Research Council of Canada and the Canadian Institute for Photonic Innovations. J. Burghoff acknowledges support by the Schott-Jenaer-Glas-Fonds.

References

1. O. Boyraz and B. Jalali, Opt. Express **12**, 5269 (2004).
2. M. A. Foster, A. C. Turner, J. E. Sharping, B. S. Schmidt, M. Lipson, and A. L. Gaeta, Nature **441**, 960 (2006).
3. L. Pavesi, L. Dal Negro, C. Mazzoleni, G. Franzo, and F. Priolo, Nature **408**, 440 (2000).
4. S. G. Cloutier, P. A. Kossyrev, and J. Xu, Nat. Mater. **4**, 887 (2005).
5. S. Furukawa and T. Miyasato, Jpn. J. Appl. Phys. Part 2 **27**, L2207 (1988).
6. L. T. Canham, Appl. Phys. Lett. **57**, 1046 (1990).
7. J. F. Morhange, G. Kanellis, and M. Balkanski, Solid State Commun. **31**, 805 (1979).
8. E. Werwa, A. A. Seraphin, L. A. Chiu, C. X. Zhou, and K. D. Kolenbrander, Appl. Phys. Lett. **64**, 1821 (1994).
9. K. M. Davis, K. Miura, N. Sugimoto, and K. Hirao, Opt. Lett. **21**, 1729 (1996).
10. E. N. Glezer and E. Mazur, Appl. Phys. Lett. **71**, 882 (1997).
11. Y. Shimotsuma, P. G. Kazansky, J. R. Qiu, and K. Hirao, Phys. Rev. Lett. **91**, 247405 (2003).
12. V. R. Bhardwaj, E. Simova, P. P. Rajeev, C. Hnatovsky, R. S. Taylor, D. M. Rayner, and P. B. Corkum, Phys. Rev. Lett. **96**, 057404 (2006).
13. A. H. Nejadmalayeri, P. R. Herman, J. Burghoff, M. Will, S. Nolte, and A. Tunnermann, Opt. Lett. **30**, 964 (2005).
14. H. Liu, G. Mourou, Y. N. Picard, S. M. Yalisove, and T. Juhasz, in *Conference on Lasers and Electro-Optics/International Quantum Electronics Conference and Photonic Applications Systems Technologies*, Technical Digest (CD) (Optical Society of America, 2004), paper CThD3.
15. H. Xia, Y. L. He, L. C. Wang, W. Zhang, X. N. Liu, X. K. Zhang, D. Feng, and H. E. Jackson, J. Appl. Phys. **78**, 6705 (1995).
16. I. Campbell, P. Fauchet, and F. Adar, Mater. Res. Soc. Symp. Proc. **53**, 311 (1986).
17. M. J. Konstantinovic, S. Bersier, X. Wang, M. Hayne, P. Lievens, R. E. Silverans, and V. V. Moshchalkov, Phys. Rev. B **66**, 161311 (2002).
18. S. Piscanec, M. Cantoro, A. C. Ferrari, J. A. Zapien, Y. Lifshitz, S. T. Lee, S. Hofmann, and J. Robertson, Phys. Rev. B **68**, 241312 (2003).